

Dynamical ion transfer between coupled Coulomb crystals in a double-well potentialAndrea Klumpp,^{1,*} Alexandra Zampetaki,¹ and Peter Schmelcher^{1,2}¹*Zentrum für Optische Quantentechnologien, Universität Hamburg, Luruper Chaussee 149, 22761 Hamburg, Germany*²*The Hamburg Centre for Ultrafast Imaging, Luruper Chaussee 149, 22761 Hamburg, Germany*

(Received 15 June 2017; published 26 September 2017)

We investigate the nonequilibrium dynamics of coupled Coulomb crystals of different sizes trapped in a double well potential. The dynamics is induced by an instantaneous quench of the potential barrier separating the two crystals. Due to the intra- and intercrystal Coulomb interactions and the asymmetric population of the potential wells, we observe a complex reordering of ions within the two crystals as well as ion transfer processes from one well to the other. The study and analysis of the latter processes constitutes the main focus of this work. In particular, we examine the dependence of the observed ion transfers on the quench amplitude performing an analysis for different crystalline configurations ranging from one-dimensional ion chains via two-dimensional zigzag chains and ring structures to three-dimensional spherical structures. Such an analysis provides us with the means to extract the general principles governing the ion transfer dynamics and we gain some insight on the structural disorder caused by the quench of the barrier height.

DOI: [10.1103/PhysRevE.96.032227](https://doi.org/10.1103/PhysRevE.96.032227)**I. INTRODUCTION**

Since their development many decades ago [1–3], ion traps have established themselves as a powerful tool in physics with applications ranging from mass spectroscopy [4,5] to high-precision tests for quantum electrodynamics [6–8] and quantum information processing [9–11].

The development of new trapping techniques, such as optical trapping [12] and the miniaturization of ion traps on chip technologies (microfabrication) [13,14] opens new possibilities for controlling the ions and accessing physically interesting and yet unexplored trapping conditions. Consequently, the experimental and theoretical understanding of the behavior of ions (both single species and mixtures) in different traps has become the focus of many recent studies [15–18].

A particular example is the study of Coulomb crystals. Using several cooling techniques, such as Doppler cooling [19,20], electromagnetically induced transparency (EIT) [21,22], or sympathetic cooling [21], it is possible to reduce the kinetic energy of the trapped particles to the regime of μK where the ions self-organize to the so-called Wigner crystals [23]. The structures of such crystals depend on the trap parameters and range from concentric rings (2D), shells (3D) [24–26], and string-of-disks configurations [27] to two-component Coulomb bicrystals [28]. By tuning the parameters of the trap potential, such as the amplitude of the AC and the amplitude and frequency of the DC potential in the case of a Paul trap or the number of ions, Wigner crystals can undergo various transitions from one structure to another [25,29]. Special attention has been given in the literature to the case of the second order phase transition from the linear to the zigzag chain of ions [30–32], which results in structures with [33–35] or without [36,37] topological defects (so-called kinks). In such a way the structural transitions of trapped ions serve among others as a playground for studying fundamental processes in physics, an example being that of the Kibble-Zurek mechanism introduced originally in the field of cosmology [34].

Given the wealth of effects resulting from a trapping of ions in an ordinary Paul trap [1], it is natural to ask for the effects stemming from a more involved trapping potential. Such a potential can be provided for ions through microfabrication, where for example segmentation can be added to the standard Paul trap [38,39] giving rise to a plethora of new possibilities for trapping potentials [11], like a double well with tunable positions of minima used for studying ion transport [40] or for splitting small ion crystals [41–44].

Focusing on the case of the double-well trapping potential, the long-range inter- and intrawell interactions among the Wigner crystals occupying each potential well give rise to a very complex nonequilibrium dynamics. In particular for a symmetric population of the two wells, we have recently shown [45] that a quench in the barrier height induces interesting non-linear dynamics, involving both regular and irregular phases of motion. Here we extend this study to the case of an asymmetric population of the double well potential. This asymmetry results in an even richer dynamics involving ion transfers between the two wells, scattering processes and crystal melting. A special focus is on the ion transfer mechanisms. We observe a nonsmooth (steplike) dependence of the time instant at which an arbitrary ion passes above the barrier on the quench amplitude, relating to the oscillation frequencies of the ion closest to the barrier, as well as to the collective center-of-mass motion of both crystals. After an ion transfer the smaller crystal melts due to the mass and energy excess a fact depicted nicely in the behavior of the so-called Voronoi measure [45,46] of the crystal.

The paper is structured as follows. In Sec. II we present the general Hamiltonian of trapped ions in the effective potential of a Paul trap, introduce our setup, and describe its ground-state configurations. Section III is divided into two parts: we first present and analyze the ion transfer processes for crystalline structures of different dimensionality and then discuss their effects on the order of the two crystals, quantified by the Voronoi measure. At the end of Sec. III we comment briefly on the possibility of realizing our setup experimentally. Finally, in Sec. IV we summarize our results and give a short outlook for further possible investigations.

*Corresponding author: aklumpp@physnet.uni-hamburg.de

II. SETUP, HAMILTONIAN, AND GROUND STATE

A. General Hamiltonian

We consider N ions, modeled as classical point particles with mass m and charge Q , confined along the radial direction (x, y) to a linear quadrupole Paul trap and along the axial direction z to a double well potential (segmented trap) [47].

The general expression for the radially confining potential $\Phi(x, y, t)$ [in the (x, y) plane] reads

$$\Phi(x, y, t) = \frac{U_{\text{dc}}}{2}(cx^2 + cy^2) + \frac{U_{\text{rf}}}{2} \cos(\omega_{\text{rf}}t)(cx^2 - cy^2), \quad (1)$$

where U_{dc} and U_{rf} are the applied constant and radiofrequency (rf) voltages, respectively; ω_{rf} denotes the (radio)frequency and c is a parameter specifying the geometry of the trap.

The ion dynamics in the radial rf trap is composed of a fast motion, the so-called micromotion, and a comparatively slow average motion ruled by an effective harmonic potential [48] $V(x, y) = \frac{m}{2}(\omega_x^2 x^2 + \omega_y^2 y^2)$. Here, $\omega_x = \frac{\omega_{\text{rf}}}{2}\sqrt{a - q^2/2}$ and $\omega_y = \frac{\omega_{\text{rf}}}{2}\sqrt{a + q^2/2}$ are the effective trapping frequencies with $a = \frac{4QU_{\text{dc}}}{m\omega_{\text{rf}}^2}c$ and $q = \frac{2QU_{\text{rf}}}{m\omega_{\text{rf}}^2}c$ being dimensionless parameters. In the following we will neglect the fast micromotion, for reasons of simplicity, being less relevant for the averaged system dynamics.

For the confinement in the z direction we assume the following phenomenological double-well potential [49]:

$$V_d(z) = \frac{m}{2}\omega_z^2 z_0^2 + \frac{m}{2}\omega_z^2 z^2 - \frac{m}{2}\sqrt{4C^2 + 4\omega_z^4 z^2 z_0^2}, \quad (2)$$

with wells centered at $\approx \pm z_0$ and separated by a barrier of height

$$B = \frac{m}{2}\left(\omega_z^2 z_0^2 + \frac{C^2}{\omega_z^2 z_0^2}\right) - mC \quad \text{with } C \in (0, \omega_z^2 z_0^2], \quad (3)$$

illustrated in Figs. 1(a) and 1(b). It can be shown that such a potential leads to individual approximately harmonic wells centered at $\approx \pm z_0$, up to terms proportional to C^2 .

Under the aforementioned assumptions, the total Hamiltonian of our system, including the radial $V(x, y)$ and the axial $V_d(z)$ trapping potentials as well as the Coulomb interactions

among the ions, reads

$$H(\{\mathbf{r}_i, \mathbf{p}_i\}) = \sum_{i=1}^n \frac{\mathbf{p}_i^2}{2m} + \sum_{i=1}^n [V_d(z_i) + V(x_i, y_i)] + \sum_{i=1, j < i}^n \frac{Q^2}{4\pi\epsilon_0 r_{ij}}, \quad (4)$$

with $\mathbf{r}_i = (x_i, y_i, z_i)$, $r_{ij} = \sqrt{(x_i - x_j)^2 + (y_i - y_j)^2 + (z_i - z_j)^2}$, and $\mathbf{p} = (p_x, p_y, p_z)$. We arrive then at the dimensionless Hamiltonian H^* by introducing rescaled time $t_u = 1/\omega_z$ and space $x_u = K \equiv [Q^2/(4\pi\epsilon_0 m\omega_z^2)]^{1/3}$ units and defining

$$t^* = \omega_z t; \quad x^* = \frac{x}{K}; \quad y^* = \frac{y}{K}; \quad z^* = \frac{z}{K}; \quad z_0^* = \frac{z_0}{K}; \\ r_{ij}^* = \frac{r_{ij}}{K}; \quad C^* = \frac{C}{K^2\omega_z^2}; \quad \alpha = \frac{\omega_x}{\omega_z}; \quad \beta = \frac{\omega_y}{\omega_z}. \quad (5)$$

Note that in the following we omit the star for simplicity and we present all our results in these dimensionless units.

B. Specific setup parameters and ground-state configurations

Having the dimensionless Hamiltonian we proceed to find its ground state (GS) configuration. Finding the global minimum of a many-ion potential is generally a highly nontrivial task. In our case, however, and for large enough values of the potential barrier B [low values of C , Fig. 1(b)], it turns out that we can find the GS configuration by using a root-finding algorithm [50], given as an initial guess the GS of the ions in two individual harmonic wells (approximating the double well potential), which is known in the literature [28,36,51–53].

Using this GS configuration as the initial state of the system, we then perform a quench in the barrier height. To analyze the nonequilibrium dynamics of the system following the quench we integrate the resulting Newtonian equations of motion (EOM) employing an implicit Gaussian fourth-order Runge-Kutta algorithm [50].

In this paper, we study a system of $N = 33$ ions confined in a combined trap with a harmonic potential in the radial direction and a double-well potential in the axial direction,

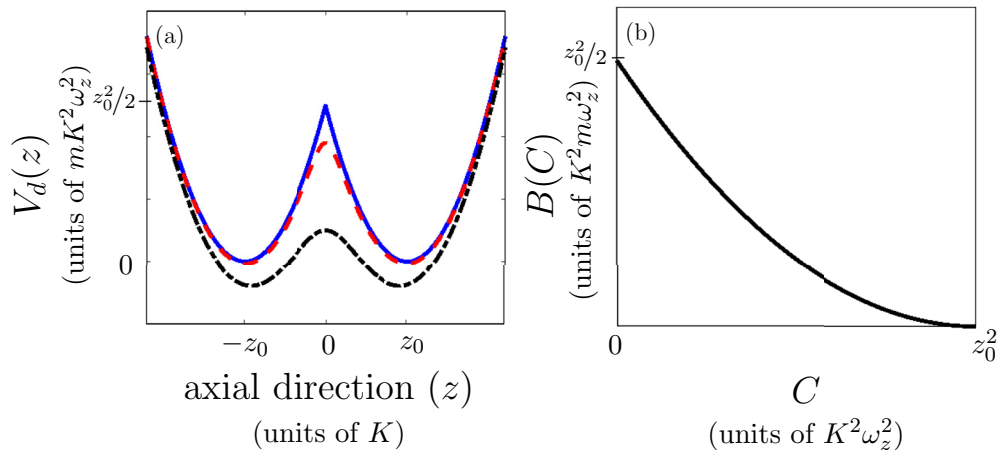


FIG. 1. (a) The double-well trapping potential in axial direction $V_d(z)$ for different values of C (blue solid line $C = 0.02$, red dashed line $C = 3$, black dashed-dotted line $C = 10$) and (b) the barrier height B as a function of C .

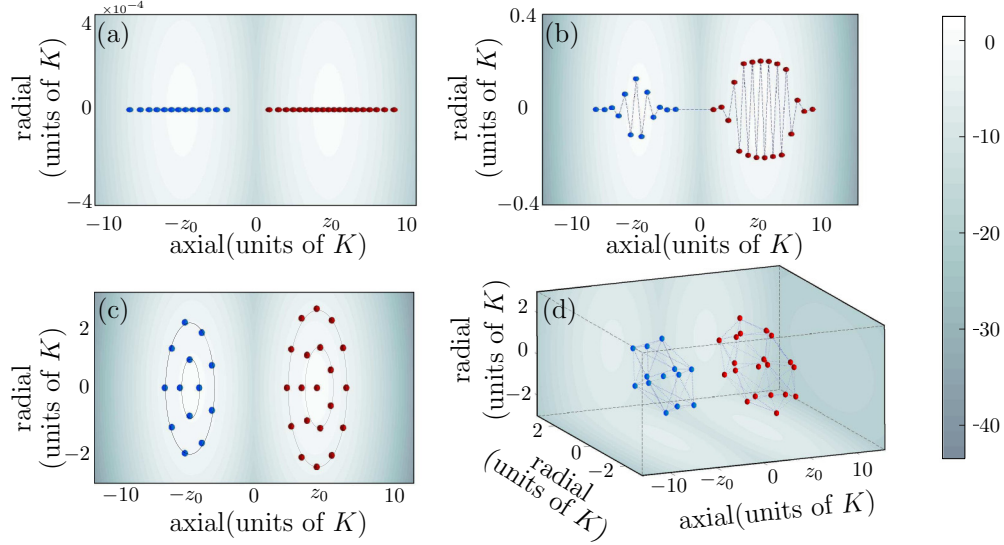


FIG. 2. Initial ion ground-state configurations for different potential parameters: (a) linear chains for $\alpha = 100$, $\beta = 100$, (b) zigzag chains for $\alpha = 5.6$, $\beta = 8$, (c) circles for $\alpha = 1$, $\beta = 8$, (d) spheres for $\alpha = 1$, $\beta = 1$. The background of the figures depicts the values of the corresponding trapping potential. All configurations and their dynamics are calculated in three dimensions with their dimensionality being restricted only by the frequency ratios α and β .

described by Eq. (4). Initially, the barrier height in the axial direction has a large value corresponding to $C_i = 0.02$ [Eq. (2), Fig. 1(a)], leading to well-separated potential wells, which are asymmetrically filled with ions, i.e., the right potential well contains $N_R = 20$ ions, whereas the left potential well contains $N_L = 13 < N_R$ ions. Regarding the radial confinement, we examine here four qualitatively different cases corresponding to different aspect ratios $\alpha = \frac{\omega_x}{\omega_z}$ and $\beta = \frac{\omega_y}{\omega_z}$ and allowing for GS configurations of different dimensionality, ranging from linear to zigzag, circular, and spherical crystals (Fig. 2). To take into account also the effect of a finite (low) temperature, we add a small random initial velocity to the ions leading to small oscillations around their GS positions.

III. ION DYNAMICS

Having described our setup allowing for a variety of equilibrium configurations (see Fig. 2), we now proceed to investigate the resulting dynamics, induced here by a change of the barrier height. In particular, we are interested in the transfer dynamics of the ions following a sudden quench of the barrier height which is characterized by the parameter C , i.e., a quench of the axial potential V_d from $C = C_i$ to $C = C_f$. We investigate therefore in the following the nonequilibrium dynamics of the Coulomb crystals in different confining potentials (Fig. 2) as a function of C_f .

With all the necessary information about the properties of our system at hand, let us now briefly introduce some of the basic features of its nonequilibrium dynamics. After a sudden quench of the barrier height, due to the energy excess, the ions constituting the Coulomb crystals start to move. Their dynamics is complex, involving among others a rather regular center of mass (CM) motion of the crystals, shock waves, multiple scattering processes, and transfer of ions over the barrier caused by the asymmetric population of the two potential wells. Especially for the cases of the circular

and spherical GS configurations also rotations and reordering of the crystals occur.

We first proceed in analyzing the ion transfer process between the two potential wells and then discuss its effects on the structure of the two Coulomb crystals.

A. Ion transfer

Among the features characterizing the ion transfer following a quench of the barrier height we are particularly interested in two aspects, to be analyzed below: the time instant at which an arbitrary ion passes above the barrier for the first time and the number of times each ion in the Coulomb crystal travels back and forth between the two wells.

Our results for the time instant of the first transfer of an arbitrary ion leaving the large crystal as a function of the final quench value C_f are presented in Fig. 3 for the different trapping geometries depicted in Fig. 2. For the facility of inspection we show only the first four traveling ions. In all the cases one can distinguish between two qualitatively different regions. The first one occupying the upper part of the plots (large transfer times $t > 10$) shows a steplike behavior (with varying C_f) consisting of small smooth regions separated by gaps, whereas the lower part (small transfer times $t < 10$) exhibits a continuous behavior. We see that depending on the value of C_f more than one ion can be transferred. Each individual ion transfer follows the same qualitative behavior with respect to its time scale. For small quench amplitudes and subsequently large transfer times the time instant of the first transfer of each ion has a steplike character, whereas beyond a certain quench amplitude the transfer time continuously decreases as a function of the final value C_f .

As a characteristic example of this behavior, without loss of generality in the remaining part of this subsection, we focus on the case of the zigzag configuration [Fig. 3(b)] and consider only the transfer of the first ion (Fig. 4). The first

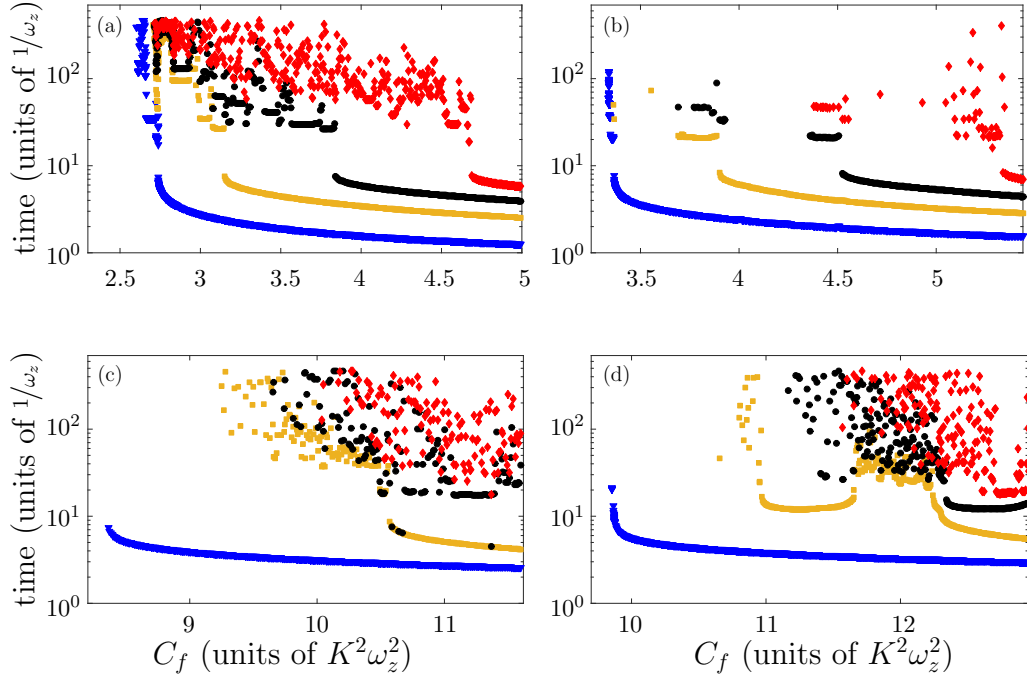


FIG. 3. Time instant of the first transfer of the first four traveling ions (order: first, blue triangle; second, yellow squares; third, black dots; fourth, red diamonds) as a function of C_f for (a) linear chains, (b) zigzag chains, (c) circles, (d) spheres. For lower C_f values than the ones depicted in the figures there is no ion transfer as explicitly shown in (a).

necessary condition for the transfer of an ion above the barrier is obviously that this ion lies close to the barrier. To examine therefore the possibility of transfer it is instructive to analyze the dynamics of the ion of the bigger crystal lying closest to the barrier, which we will refer to in the following as the innermost ion. Such an analysis can be facilitated by examining a case in which ion transfer although energetically possible does not occur, i.e., corresponding to a quench value inside a gap of Fig. 4. A case satisfying these criteria and consequently

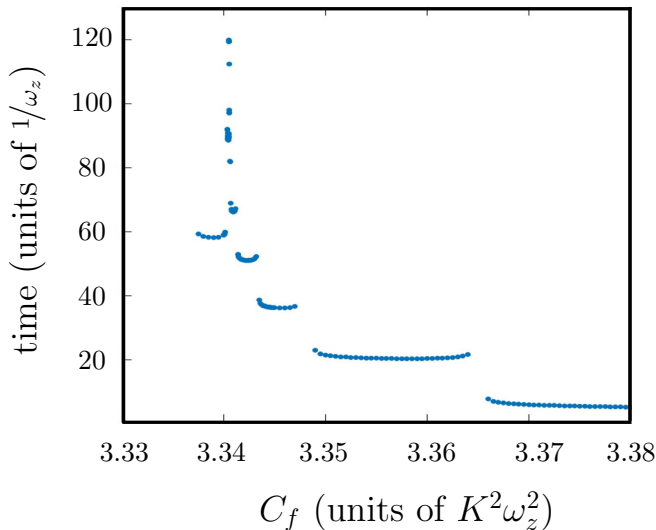


FIG. 4. Time instant of the first transfer of the first traveling ion as a function of C_f for the case of the zigzag chain [zoom of Fig. 3(b)].

allowing for an analysis of the long-time dynamics of the innermost ion without interruptions by ion transfer processes is that of a final quench value $C_f = 3.3403$.

The time evolution of the axial position of the innermost ion of the large crystal for $C_f = 3.3403$, as well as its Fourier spectrum are shown in Fig. 5. The motion appears to be oscillatory and quite regular with one dominant frequency, a fact supported also by the Fourier spectrum which shows essentially the contribution of three frequencies, with one of them possessing a dominant role (largest amplitude). To test whether this frequency is generic for our system, we have investigated the Fourier spectra of the innermost ion motion for four different values of C_f , which do not lead to transfer. The results are depicted in Fig. 6. Obviously in all the cases there is one predominant frequency in the range of $\omega \approx 0.84$ to 0.88 , which in turn yields a period T ranging approximately from 7.1 to 7.4 . A comparison of this period with the time between the subsequent steps in Fig. 4 leads to the conclusion that the latter is equal to one or two times the period T (Fig. 7) within a range of 3.5% . This fact explains the existence of the steps in the ion transfer process as a direct consequence of a preferred oscillation phase (closest to the barrier) of the innermost ion. What remains to be answered is why not every time separation equal to the period T leads to transfer and why some time separations between the steps are two times the period T , i.e., some steps are absent.

To provide an answer to this question it is essential to take into account also the dynamics of the other ions constituting the Coulomb crystals.

After the quench all ions constituting the two Coulomb crystals move towards the barrier, as it can be seen by inspecting their CM motion [Fig. 8(a)]. Since the two crystals

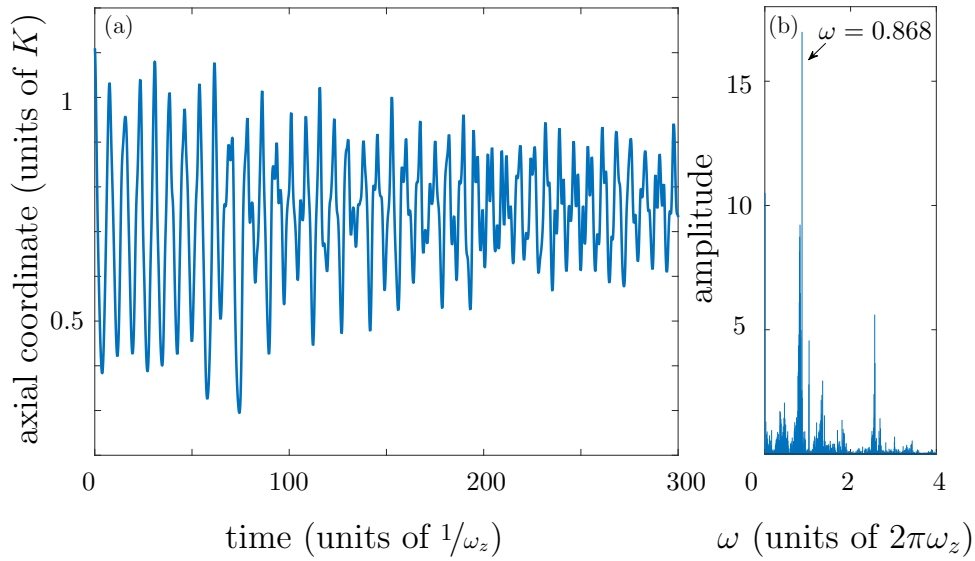


FIG. 5. The axial motion of the innermost ion of the zigzag configuration and its Fourier spectrum for $C_f = 3.3403$.

interact via repulsive Coulomb forces, the repulsion exerted by the small crystal hinders the transfer of the innermost ion of the large crystal. If the energy introduced by the quench is high enough to overcome the Coulomb interaction and the barrier, the innermost ion travels, otherwise the two crystals start to oscillate without any ion transfer, as depicted in their CM dynamics [Fig. 8(a)]. The Fourier analysis of this CM motion shows that the frequencies of the left and right crystals differ [Fig. 8 (b)] due to their different sizes. Therefore, there is a variety of possibilities for the position of the two crystals during the time evolution [see Fig. 8(a)]: (i) they can both be close to the barrier [line A in Fig. 8(a)], (ii) both can be far away from the barrier [line B in Fig. 8(a)], (iii) the large crystal can be close to the barrier and the small far away [line C in Fig. 8(a)], or (iv) the opposite of (iii) [line D in Fig. 8(a)]. Obviously, the case with the small crystal being far and the large crystal being close to the barrier (case C) is optimal for the transfer, both in terms of energy and spatial configuration.

It turns out that the two CM frequencies depend also on the value of the barrier height, thus the time instant when the optimal conditions are fulfilled changes slightly with

C_f , leading to different times for ion transfer appearing as different steps in Fig. 7. In the same line of arguments, it is possible, depending on C_f , that the innermost ion is close to the barrier when the CM of the larger crystal is not and thus due to the lack of energy the ion transfer is prohibited, leading to some steps being skipped and the subsequent steps appearing after a time $2T$ (Fig. 7). In Fig. 8(b), we also see that apart from the main frequencies ω_p for the two crystals, there also exist additional beating frequencies ω_b . This results in an amplitude modulation [see Fig. 8(a)], which also influences the transfer dynamics. Interestingly enough, the pairs of ω_p, ω_b frequencies for the small and the large crystal are approximately degenerate, a fact that could be attributed to their Coulomb coupling.

Another feature of the CM dynamics is the damping of the oscillations of the big crystal with time [Fig. 8(a), lines E], limiting the time available for ion transfer and giving rise to the observed gaps of Figs. 3 and 4. The origins of this damping are the repulsive interactions between the two crystals, the transfer of energy in the radial directions (here

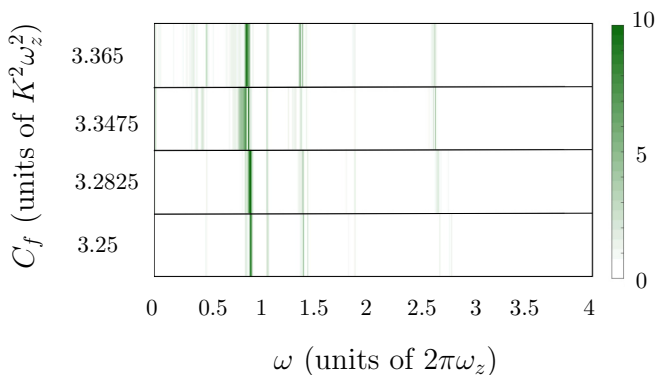


FIG. 6. Comparison of the Fourier spectra of the innermost ion motion for four different values of C_f . The color depicts their amplitude.

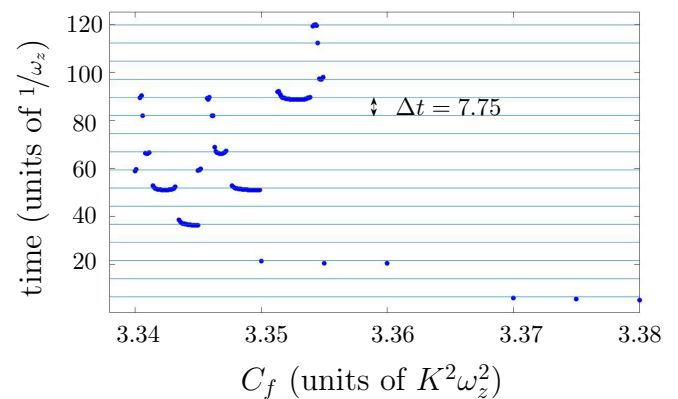


FIG. 7. The time instant for the first transfer of the innermost ion as a function of C_f for the zigzag configuration. The horizontal lines mark the multiples of the period T of the innermost ion.

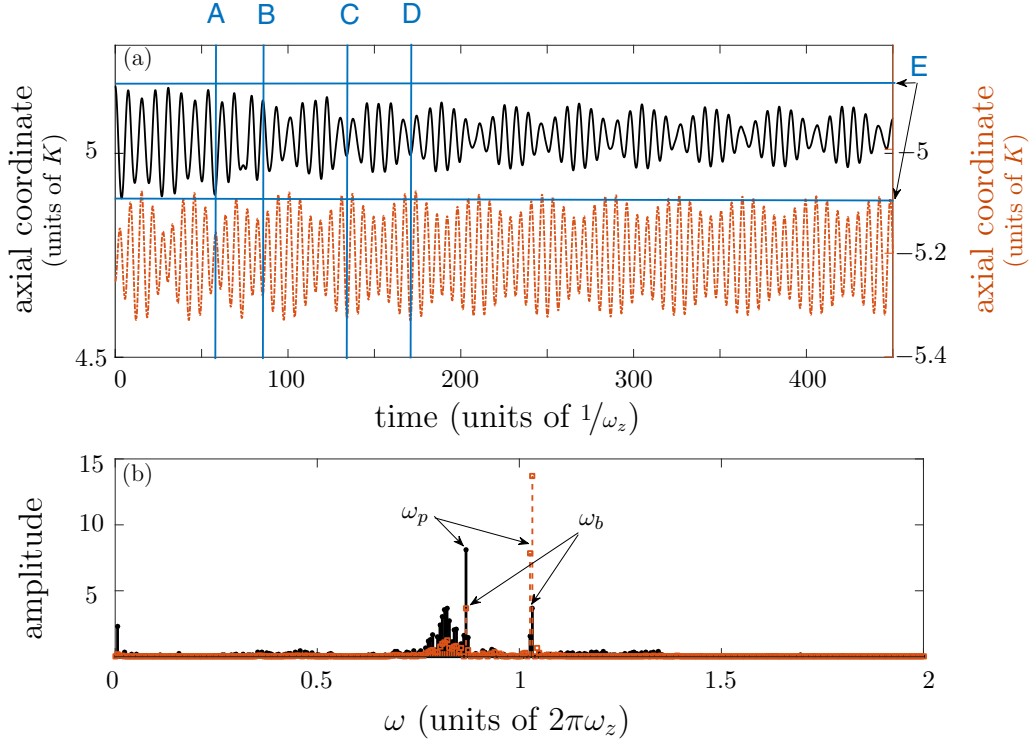


FIG. 8. (a) CM motion of the two crystals (large crystal, solid black line; small crystal, red dashed line) for the zigzag configuration with $C_f = 3.3403$. The vertical lines A, B, C, and D mark the time instants during the dynamics corresponding to qualitatively different positions of the two Coulomb crystals. The horizontal lines E denote the initial amplitude of the CM motion of the large crystal. (b) The corresponding Fourier spectra for the large (black, $\omega_p = 0.868$ and $\omega_b = 1.0264$) and the small crystal (dashed red with squares, $\omega_p \approx 1.0323$ and $\omega_b \approx 0.868$).

especially in the less confining direction), and the mode coupling between the CM modes and other modes, due to the inherent nonlinearity of the system.

In contrast to the above discussion, if the energy introduced by the quench is large enough, the details of the dynamics of the CM motion seize to rule the transfer process of an ion, resulting in a smooth behavior of the time instant for an ion to cross the barrier as a function of C_f (Fig. 3).

So far we have focused on the first time instant at which an ion is transferred from one well to the other. But as already mentioned, an ion can travel back and forth thereby passing the potential barrier several times. To extract information on the number of transfers per ion, we have sorted the ions in their initial GS configuration according to their positions in the axial direction in increasing order and we have counted for each one the number of transfers occurring in the time interval considered for the dynamical evolution. Using this convention, the first 13 ions are at $t = 0$ in the small and the next 20 in the big crystal. In Fig. 9, the results for the different initial configurations (Fig. 2) are shown.

We have already seen (Fig. 3) that for the linear and the zigzag configurations, in the considered region of C_f , only five ions travel. These are the ions that are located in the big crystal closest to the barrier (ion numbers 14 to 19). As we observe [Figs. 9(a) and 9(b)] these five ions travel several times forth and back over the barrier during our simulation time, whereas none of the other ions in the two crystals ever crosses the barrier. The reason for this is the strict confinement in the radial direction for these two cases, which is especially

true for the linear chains. For the zigzag case, as long as the ion order in the axial direction is preserved the exclusive transfer of only five ions also holds, but for larger values of $C_f > 6.5$ (where the strict axial order is destroyed), further ions do also get the possibility of being transferred [compare Fig. 9(b)].

In contrast to the above, for the cases of the circle and sphere configurations [Figs. 9(c) and 9(d)] all ions can be transferred. The low aspect ratios ($\alpha = 1$) of the radial confining potentials of the circle and the spherical configurations enable rotations of the whole crystals, as well as rearrangements with respect to the order of the ions constituting them. Thus, in the course of the dynamics, the order of the ions in the axial direction changes and different ions are located at different times closer to barrier, resulting for larger C_f in a nearly uniform distribution of the number of transfers among the ions of the two crystals. Having understood the basic features of the ion transfer processes, let us now examine how these do affect the order and the structure of the two involved Coulomb crystals.

B. Crystalline order

The ion transfer processes discussed above yield a complex nonequilibrium dynamics of the two resulting Coulomb crystals involving reordering processes and the emergence of structural disorder. To characterize and analyze the order of the resulting crystals we make use of a measure based on the Voronoi diagrams introduced in Refs. [45,46]. A Voronoi diagram partitions a given region into subsets, based on the distance of each point in the region from particular points that are called seeds (here these correspond to the positions

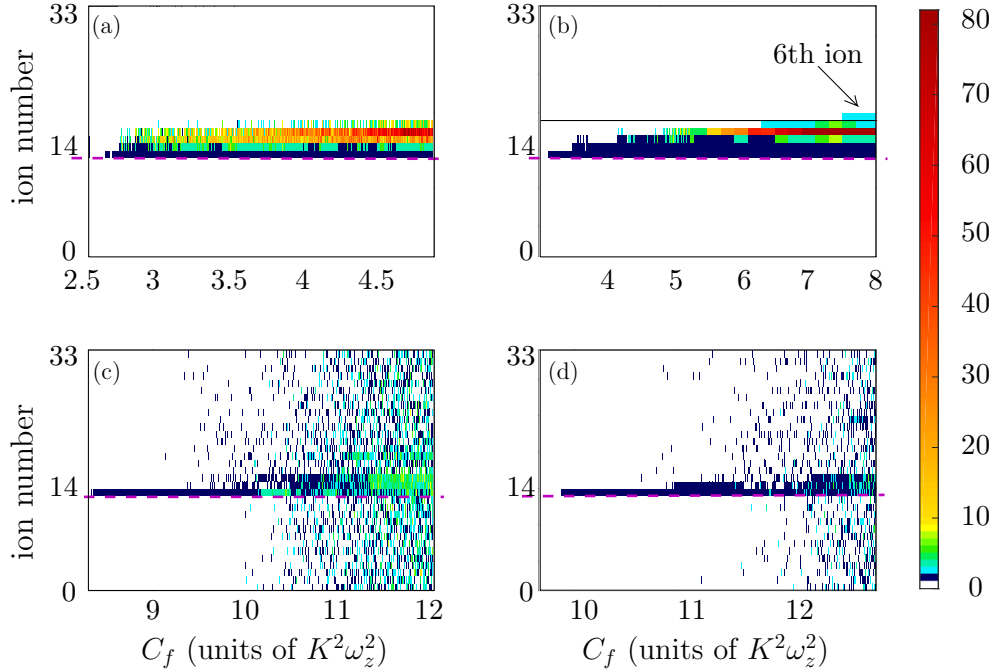


FIG. 9. Number of transfers per ion as a function of C_f for (a) linear chains, (b) zigzag chains, (c) circles, (d) spheres. The (pink) dashed line separates the ions of the small from the ions of the large crystal.

of the ions). Each subset assigned to a specific seed (Voronoi cell) constitutes a region consisting of all points closer to that seed than to any other. The Voronoi cells in the d -dimensional Euclidean space possess, in general, an arbitrary polyedric shape. Of particular importance is the minimum distance of the seed from any side of this polyedron. Using this as a radius we can construct a d -dimensional sphere assigned to each seed, termed here as Voronoi sphere. The sizes of these Voronoi spheres can be used to characterize effects such as clustering through the so-called Voronoi measure. This measure is constructed by summing the d -dimensional volumes of all the Voronoi spheres. Interestingly, the time evolution of this measure has been proven to capture well the change in the crystalline order of Coulomb crystals during dynamics [45], a fact that justifies its use also in the current work.

In the specific setup we study here, the two Coulomb crystals have different sizes causing them to behave differently. For each crystal located in a certain well we determine its Voronoi measure value, taking also into account that the number of ions per well (crystal) changes in time due to the ion transfer processes. Considering also the factor of dimensionality we arrive at the following definition of our Voronoi measure Ω ,

$$\Omega(t) = \gamma \frac{1}{N} \sum_i \left(\frac{r_{ij}(t)}{2} \right)^d, \quad (6)$$

where N is the number of ions in the well and r_{ij} is the distance of each particle i from its nearest neighbor j . Therefore, for our setup this measure corresponds to the sum of the volumes of spheres centered in each ion i , with a diameter equal to r_{ij} (Voronoi spheres), i.e., the sum of volumes in which only one

ion can be found (see Fig. 10). The variables d and γ depend on the dimensionality of the configurations. For the linear chains (1D) we have that $d = 1$ and $\gamma = 1$, for the zigzag chains and the circular structures (2D) $d = 2$ and $\gamma = \pi$ and for the spherical configurations $d = 3$ and $\gamma = 4\pi/3$.

In the course of the dynamics the system of ions alternates between clustered and dispersed ion configurations resulting in an alternating Voronoi measure. The clustered structures that in most cases give visually the impression of order lead to low values in the time evolution of the Voronoi measure, whereas a scattered distribution of the ions leads to larger values of $\Omega(t)$ [45].

An example of the time evolution of the Voronoi measure $\Omega(t)$ after the quench of the barrier height is shown in Fig. 11(a)

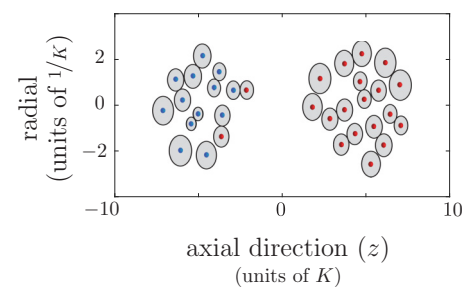


FIG. 10. Snapshots of the ion dynamic (blue dots, initial position of the ion is in the small crystal; red dots, initial position is in the big crystal) and the respective Voronoi spheres (gray circles) used to calculate the Voronoi measure. Here the trapping parameters are chosen so that the two crystals self-organize in circular shells [see Fig. 2 (c)]. The snapshots correspond to a value $\Omega = 2.85$ for the left and $\Omega = 3.35$ for the right well.

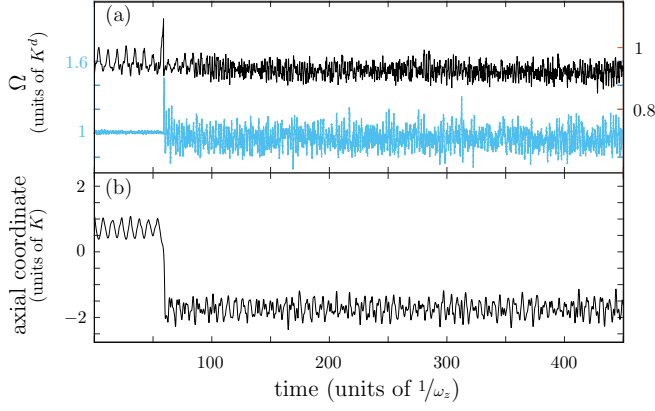


FIG. 11. The time evolution of (a) the Voronoi measure (Ω) of the two ion crystals [large ion crystal, black; small ion crystal, light blue (gray)] and (b) the axial position of the innermost ion for the zigzag configuration and $C_f = 3.34$.

for the zigzag Coulomb crystals [Fig. 2(b)] and for the final quench value $C_f = 3.34$ for which a single ion is transferred at $t \approx 59$ [Figs. 3(b) and 4]. For comparison we also present the time evolution of the axial coordinate of the traveling ion [Fig. 11(b)]. We observe that initially (i.e., before the ion transfer) the Voronoi measure exhibits regular oscillations with a much larger amplitude for the large crystal compared to the smaller one. This can be attributed to the larger shell diameter of the former, which allows for larger deformations (i.e., compressions and expansions).

At the time instant when the ion crosses the barrier [Fig. 11(b)] the Voronoi values of both the large and the small crystal exhibit a prominent peak [Fig. 11(a)] resulting from the change in the number of ions per crystal and the fact that the distance of the traveling ion from its nearest neighbors maximizes when it crosses the barrier. After the ion transfer the Voronoi measure of the small crystal performs highly irregular oscillations with an increased amplitude, pointing to the irregular and disordered dynamics of the ions constituting the crystal (crystal melting). In contrast, the oscillation amplitude of the Voronoi measure for the large crystal decreases slightly after the ion transfer due to the increment of available space for the ion dynamics and the substantial loss of energy caused by the loss of the highly energetic traveling ion. Similarly to the case of the smaller crystal the oscillations after the transfer become more irregular involving multiple frequencies.

These results suggest that the Voronoi measure $\Omega(t)$ and especially its oscillation amplitude encapsulates substantial information on the out-of-equilibrium many-body ion dynamics following the quench of the barrier height. Nevertheless, to proceed to an analysis of the crystalline order as a function of the final quench parameter C_f we would like to have a single value characterizing each time series. A measure related closely to the average oscillation amplitude of $\Omega(t)$ (i.e., capturing well the average dynamics of the crystals) is its standard deviation $\Delta\Omega$ in time. The larger the value of $\Delta\Omega$, the stronger the fluctuations in the Voronoi measure $\Omega(t)$; i.e., the ion structures alternate strongly between clustered and dispersed.

The resulting values for the standard deviations $\Delta\Omega$ as a function of C_f are shown in Fig. 12 for the different

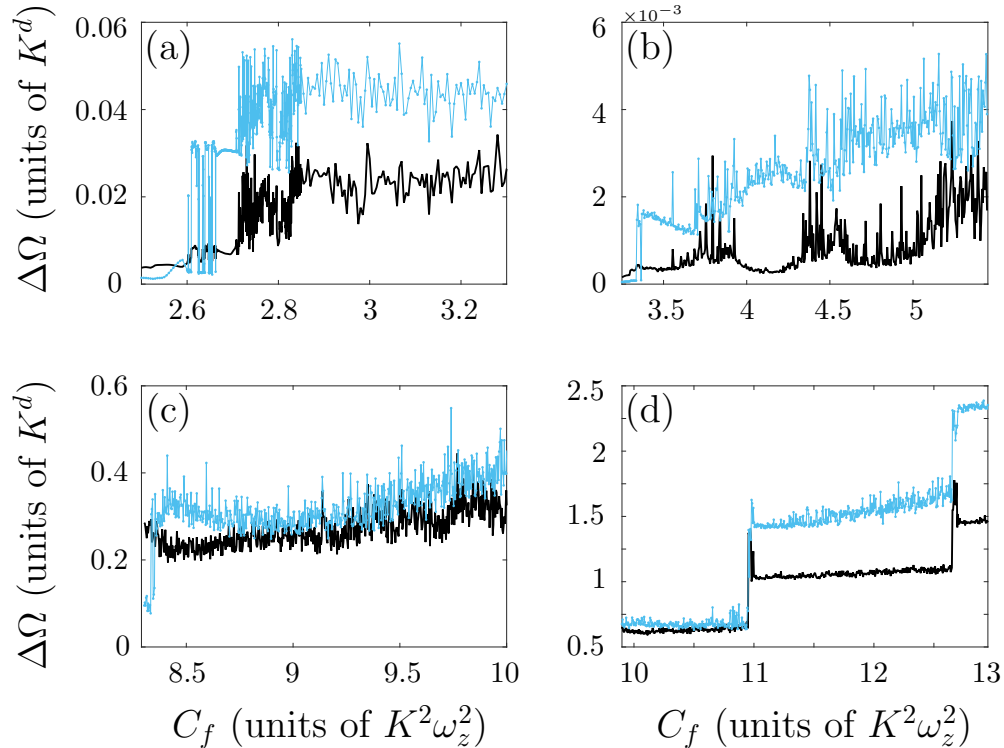


FIG. 12. Standard deviation of Ω as a function of C_f for (a) linear chain, (b) zigzag, (c) circle, and (d) sphere configurations [black line for the large and light blue (gray) line for the small crystal].

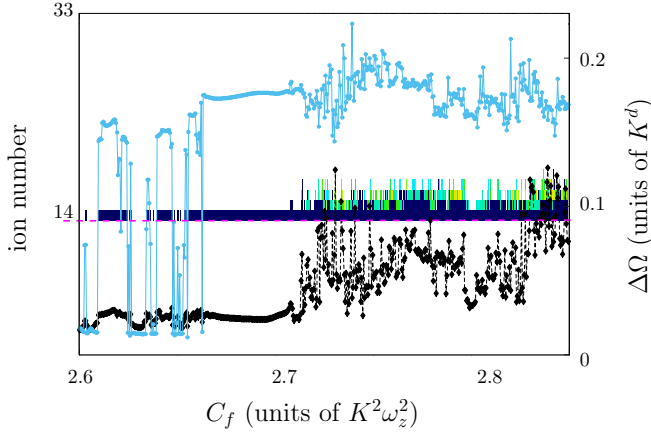


FIG. 13. Standard deviation and number of transfers per ion for the linear chain configuration in the range $C_f \in [2.6, 2.85]$ [black dashed line with diamonds for the large crystal and light blue (gray) line with dots for the small crystal].

trapping potentials examined (Fig. 2). The standard deviation $\Delta\Omega$ for the one [Fig. 12(a)] and two-dimensional [Figs. 12(b) and 12(c)] ion configurations are highly irregular but for the three-dimensional configuration [Fig. 12(d)] it is rather well structured, giving immediate access to relevant information.

Focusing on the noisy character encountered, for example, in the case of the linear chain, it turns out that many ion transfer processes occur. This can be inferred by an inspection of Fig. 13, where the behavior of $\Delta\Omega$ is compared to that of the number of transfers per ion as a function of C_f in the interval $C_f \in [2.6, 2.85]$. Clearly every small change in the transfer dynamics results in a substantial change in the standard deviation of the Voronoi measure $\Delta\Omega$, yielding the highly irregular pattern of the latter.

For the zigzag and the circle configurations [Figs. 12(b) and 12(c)], although there are intervals of $\Delta\Omega$ exhibiting a relatively smooth behavior as a function of C_f (especially for lower values of C_f) the overall pattern is quite noisy as well resembling the case of the linear chain [Figs. 12(a) and 13]. In direct contrast, in the case of the spherical configuration [Fig. 12(d)] we observe a rather regular behavior of $\Delta\Omega$ as a function C_f , allowing for extracting more directly information regarding the order of the Coulomb crystals involved.

Note here that among others the Voronoi measure and its standard deviation depend also on the dimensionality of the configurations [Eq. (6)] and the space available for motion. Therefore, as it is obvious [Fig. 12(d)], the values of $\Delta\Omega$ for the three-dimensional configuration (spheres), where the available volume for the corresponding motion is much more enhanced, are orders of magnitude larger than that for the cases of lower dimensionality [Figs. 12(a)–12(c)]. This results in the former being less sensitive to small deviations yielding the overall regular pattern of $\Delta\Omega$ for the case of spheres.

In particular, we observe that $\Delta\Omega$ exhibits a quite smooth step-like behavior interrupted by pronounced peaks as C_f increases. To understand this behavior we compare it to the C_f dependence of the two quantities characterizing the ion transfer: the number of times each ion in the Coulomb crystal travels back and forth between the two potential wells [Fig. 14(a)] and the time instant at which an arbitrary ion passes above the barrier for the first time [Fig. 14(b)]. We observe that at most C_f values for which an additional ion transfer occurs the standard deviation of the Voronoi measure $\Delta\Omega$ possesses a peak, followed thereafter by the steplike behavior of the other quantities [Figs. 14(a) and 14(b)]. This can be interpreted as an increment of the structural disorder in the two crystals induced by the increasing amount of ion transfer processes and maximized each time a new ion gets transferred.

C. Possible experimental realization

Let us finally address the experimental realization of our setup, employing state-of-the-art ion technology. Typical experimental parameters for segmented Paul traps are $\omega_{rf}/2\pi = 4.2\text{--}50$ MHz and $U_{rf} = 8\text{--}350$ V with applied DC voltages in the axial direction up to 10 V [42,54]. Depending on the ion species and trap design these result in a radial confinement frequency $\omega/2\pi = 1\text{--}5$ MHz and in an axial confinement frequency $\omega_z/2\pi = 0\text{--}5$ MHz. For the ion dynamics only the frequency ratio $\alpha = \frac{\omega}{\omega_z}$ matters and given the aforementioned frequency ranges the scenario studied in this work of $\alpha = 8.25$ could be in principle realized (choosing, e.g., $\omega/2\pi = 4.5$ MHz and $\omega_z/2\pi = 0.545$ MHz). The parameters z_0 and C , determining the well positions and the barrier height, respectively, depend on the axial DC voltage and the trap geometry, thus realistic values for the former are of the order of

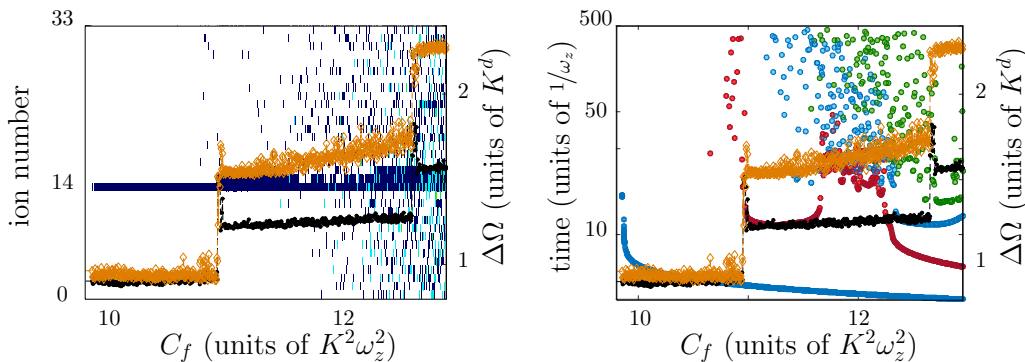


FIG. 14. Standard deviation of the spherical configuration [black line with dots for the large and orange (gray) line with diamonds for the small crystal] combined with (a) the number of transfers per ion and (b) the time instant of the first transfer of ions (for the first four traveling ions marked with dots of different colors).

30 μm and for the latter up to 300 $\mu\text{m}^2 \cdot \text{MHz}^2$. Regarding the imaging of the ion configurations during their non-equilibrium dynamics, this could be achieved by the use of fluorescence light detected by CCD cameras [33,42].

IV. CONCLUSIONS

We have explored the nonequilibrium dynamics of two Coulomb crystals of different sizes occupying the individual wells of a double-well potential, following a quench of the potential barrier height. The resulting complex dynamics is governed by ion transfer processes from one well to the other, depending on the quench amplitude.

The time instant at which an arbitrary ion passes the barrier for the first time shows an interesting steplike behavior as a function of the quench amplitude. By analyzing the crystal dynamics we were able to explain the main features of this dependence. It turns out that the most crucial quantities determining whether ion transfer finally occurs are the center of mass motions of both crystals and the oscillation frequencies of the innermost ion.

Following the ion transfer the dynamics of the two crystals becomes rather irregular and characterized by structural disorder as well as reordering of the particles. A good quantity

to characterize the crystalline order is the so-called Voronoi measure. Its standard deviation in time reflects well the degree of the structural disorder resulting from the quench and serves as a good indicator for the ion transfer processes.

A future work could investigate the case of two Coulomb crystals (with or without kinks), separated by a potential barrier, and aim at achieving a transport of medium-sized crystals (i.e., 10–100 ions). Another promising direction for future research is the nonequilibrium dynamics of Coulomb crystals in multiple-well potentials resembling the optical lattices used in studies of ultracold atoms. Finally, although for our setup in the parameter regime studied here quantum effects are negligible, an investigation of them for parameters allowing the system to exhibit its quantum character would also be of interest. It is expected that in such a case quantum tunneling below barrier would add to the classical ion transfer shown here, giving rise to an even richer nonequilibrium dynamics.

ACKNOWLEDGMENTS

We thank B. Liebchen for useful discussions and suggestions. A.K. thanks S. Klumpp for scientific discussions and support.

-
- [1] W. Paul and H. Steinwedel, *Z. Naturforschg. A* **8**, 448 (1953).
 - [2] F. Penning, *Physica* **3**, 873 (1936).
 - [3] H. Dehmelt, *Rev. Mod. Phys.* **62**, 525 (1990).
 - [4] P. H. Dawson, *Int. J. Mass Spectrom. Ion Phys.* **21**, 317 (1976).
 - [5] R. E. March and J. F. Todd, *Practical Aspects of Ion Trap Mass Spectrometry: Chemical, Environmental, and Biomedical Applications*, Vol. 3 (CRC Press, Boca Raton, FL, 1995).
 - [6] A. Kreuter, C. Becher, G. P. T. Lancaster, A. B. Mundt, C. Russo, H. Häffner, C. Roos, J. Eschner, F. Schmidt-Kaler, and R. Blatt, *Phys. Rev. Lett.* **92**, 203002 (2004).
 - [7] M. Steiner, H. M. Meyer, C. Deutsch, J. Reichel, and M. Köhl, *Phys. Rev. Lett.* **110**, 043003 (2013).
 - [8] G. Guthohriein, M. Keller, K. Hayasaka, W. Lange, and H. Walther, *Nature* **414**, 49 (2001).
 - [9] J. I. Cirac and P. Zoller, *Phys. Rev. Lett.* **74**, 4091 (1995).
 - [10] D. J. Wineland, C. Monroe, W. M. Itano, D. Leibfried, B. E. King, and D. M. Meekhof, *J. Res. Natl. Inst. Stan.* **103**(3), 259 (1998).
 - [11] D. Kielpinski, C. Monroe, and D. J. Wineland, *Nature* **417**, 709 (2002).
 - [12] C. Schneider, M. Enderlein, T. Huber, and T. Schaetz, *Nat. Photon.* **4**, 772 (2010).
 - [13] M. D. Hughes, B. Lekitsch, J. A. Broersma, and W. K. Hensinger, *Contemp. Phys.* **52**, 505 (2011).
 - [14] G. Wilpers, P. See, P. Gill, and A. G. Sinclair, *Nat. Nanotechnol.* **7**, 572 (2012).
 - [15] A. Härter and J. H. Denschlag, *Contemp. Phys.* **55**, 33 (2013).
 - [16] W. W. Smith, O. P. Makarov, and J. Lin, *J. Mod. Opt.* **52**, 2253 (2005).
 - [17] A. T. Grier, M. Cetina, F. Oručević, and V. Vuletić, *Phys. Rev. Lett.* **102**, 223201 (2009).
 - [18] C. Champenois, *J. Phys. B: At. Mol. Opt.* **42**, 154002 (2009).
 - [19] D. J. Wineland and W. M. Itano, *Phys. Rev. A* **20**, 1521 (1979).
 - [20] W. Neuhauser, M. Hohenstatt, P. Toschek, and H. Dehmelt, *Phys. Rev. Lett.* **41**, 233 (1978).
 - [21] G. Morigi, J. Eschner, and C. H. Keitel, *Phys. Rev. Lett.* **85**, 4458 (2000).
 - [22] G. Morigi, *Phys. Rev. A* **67**, 033402 (2003).
 - [23] E. Wigner, *Phys. Rev.* **46**, 1002 (1934).
 - [24] J. J. Bollinger, D. J. Wineland, and D. H. E. Dubin, *Phys. Plasm.* **1**, 1403 (1994).
 - [25] D. H. E. Dubin and T. M. O'Neil, *Rev. Mod. Phys.* **71**, 87 (1999).
 - [26] M. Bonitz, P. Ludwig, H. Baumgartner, C. Henning, A. Filinov, D. Block, O. Arp, A. Piel, S. Käding, Y. Ivanov, A. Melzer, H. Fehske, and V. Filinov, *Phys. Plasm.* **15**, 055704 (2008).
 - [27] N. Kjærgaard and M. Drewsen, *Phys. Rev. Lett.* **91**, 095002 (2003).
 - [28] L. Hornekær, N. Kjærgaard, A. M. Thommesen, and M. Drewsen, *Phys. Rev. Lett.* **86**, 1994 (2001).
 - [29] G. Birkl, S. Kassner, and H. Walther, *Nature* **357**, 310 (1992).
 - [30] G. Morigi and S. Fishman, *Phys. Rev. Lett.* **93**, 170602 (2004).
 - [31] G. Morigi and S. Fishman, *Phys. Rev. E* **70**, 066141 (2004).
 - [32] J. D. Baltrusch, C. Cormick, and G. Morigi, *Phys. Rev. A* **86**, 032104 (2012).
 - [33] M. Mielenz, J. Brox, S. Kahra, G. Leschhorn, M. Albert, T. Schaetz, H. Landa, and B. Reznik, *Phys. Rev. Lett.* **110**, 133004 (2013).

- [34] K. Pyka, J. Keller, H. Partner, R. Nigmatullin, T. Burgermeister, D. Meier, K. Kuhlmann, A. Retzker, M. Plenio, W. Zurek, A. del Campo, and T. Mehlstaubler, *Nat. Commun.* **4**, 2291 (2013).
- [35] S. Ulm, J. Ronagel, G. Jacob, C. Degünther, S. T. Dawkins, U. G. Poschinger, R. Nigmatullin, A. Retzker, M. B. Plenio, and F. S.-K. K. Singer, *Nat. Commun.* **4**, 2290 (2013).
- [36] D. H. E. Dubin, *Phys. Rev. Lett.* **71**, 2753 (1993).
- [37] S. Fishman, G. De Chiara, T. Calarco, and G. Morigi, *Phys. Rev. B* **77**, 064111 (2008).
- [38] S. A. Schulz, U. G. Poschinger, F. Ziesel, and F. Schmidt-Kaler, *New J. Phys.* **10**, 045007 (2008).
- [39] U. Tanaka, K. Suzuki, Y. Ibaraki, and S. Urabe, *J. Phys. B* **47**, 035301 (2014).
- [40] G. Huber, T. Deuschle, W. Schnitzler, R. Reichle, K. Singer, and F. Schmidt-Kaler, *New J. Phys.* **10**, 013004 (2008).
- [41] T. Ruster, C. Warschburger, H. Kaufmann, C. T. Schmiegelow, A. Walther, M. Hettrich, A. Pfister, V. Kaushal, F. Schmidt-Kaler, and U. G. Poschinger, *Phys. Rev. A* **90**, 033410 (2014).
- [42] H. Kaufmann, T. Ruster, C. Schmiegelow, F. Schmidt-Kaler, and U. Poschinger, *New J. Phys.* **16**, 073012 (2014).
- [43] M. Barrett, J. Chiaverini, T. Schaetz, J. Britton, W. Itano, J. Jost, E. Knill, C. Langer, D. Leibfried, R. Ozeri, and D. J. Wineland, *Nature* **429**, 737 (2004).
- [44] M. A. Rowe, A. Ben-Kish, B. DeMarco, D. Leibfried, V. Meyer, J. Beall, J. Britton, J. Hughes, W. M. Itano, B. Jelenković, C. Langer, T. Rosenband, and D. J. Wineland, *Quant. Inf. Comp.* **2**, 257 (2002).
- [45] A. Klumpp, B. Liebchen, and P. Schmelcher, *Phys. Lett. A* **380**, 2644 (2016).
- [46] F. P. Preparata and M. I. Shamo, *Computational Geometry* (Springer Verlag, New York, 1985).
- [47] The combination of the linear quadrupole trap potential and a double-well potential is not allowed by the Laplace equation. Therefore, it would be necessary to compensate for it by a complex form of the dc part in the radial direction. In recent experiments with segmented Paul traps (e.g., Refs. [55,56]) this combination was realized, giving rise to a potential similar to the one we have chosen here as well as to a Mexican hat-like potential.
- [48] D. Gerlich, in *State-Selected and State-to-State Ion-Molecule Reaction Dynamics, Part 1. Experiment*, Advances in Chemical Physics, edited by C.-Y. Ng and M. Baer, Vol. 82 (John Wiley & Sons, Inc., 1992), pp. 1–176.
- [49] A. I. Streltsov, O. E. Alon, and L. S. Cederbaum, *Phys. Rev. A* **73**, 063626 (2006).
- [50] M. Galassi, J. Davis, J. Theiler, B. Gough, G. Jungman, P. Alken, M. Booth, and F. Rossi, *GNU Scientific Library Reference Manual*, 3rd ed., edited by B. Gough (Network Theory Ltd., 2009).
- [51] M. Drewsen, I. S. Jensen, N. Kjærgaard, J. Lindballe, A. Mortensen, K. Mølhave, and D. Voigt, *J. Phys. B: At. Mol. Opt. Phys.* **36**, 525 (2003).
- [52] V. M. Bedanov and F. M. Peeters, *Phys. Rev. B* **49**, 2667 (1994).
- [53] P. Ludwig, S. Kosse, and M. Bonitz, *Phys. Rev. E* **71**, 046403 (2005).
- [54] W. K. Hensinger, S. Olmschenk, D. Stick, D. Hucul, M. Yeo, M. Acton, L. Deslauriers, C. Monroe, and J. Rabchuk, *Appl. Phys. Lett.* **88**, 034101 (2006).
- [55] K. R. Brown, C. Ospelkaus, Y. Colombe, A. C. Wilson, D. Leibfried, and D. J. Wineland, *Nature* **471**, 196 (2011).
- [56] M. Harlander, R. Lechner, M. Brownnutt, R. Blatt, and W. Hänsel, *Nature* **471**, 200 (2011).